Coupled topological interface states

Christoph Schmidt,* Alexander Palatnik, Markas Sudzius, Stefan Meister, and Karl Leo†
Dresden Integrated Center for Applied Physics and Photonic Materials, Technische Universität Dresden, 01187 Dresden, Germany

(Received 28 August 2020; accepted 19 January 2021; published 8 February 2021)

Topological interface states in one-dimensional electronic and photonic systems are currently intensively investigated. We demonstrate the coupling of topologically confined states: By concatenation of three substructures, where the outer embedding structures have opposite signs of reflection phases to the embedded structure, we realize a system of coupled interface states showing mode splitting. We theoretically and experimentally show that a topological transition occurs for this coupled system. The demonstration of these systems is put on a solid foundation by first realizing the substructures relevant for interface states between topologically distinct one-dimensional photonic crystals. We experimentally demonstrate band closing and band inversion for a redistribution of the optical path to the constitutive materials of the structures. The band inversion is demonstrated by the emergence of interface states at metal-dielectric interfaces and the findings are supported by ellipsometric measurements.

DOI: 10.1103/PhysRevB.103.085412

I. INTRODUCTION

The connection of topology and condensed matter physics led to exciting new physics such as the quantum spin Hall effect [1,2] and topological insulators [3]. It was soon realized that the formalism can also be applied to photonics [4], creating topological photonics, a now rapidly developing field [5,6]. The mathematical equivalence of some forms of Maxwell's equations in an operator theory approach to the mathematical formalism of quantum mechanics allows one to adopt results from condensed matter physics [7]. For example, paraxial propagation of light in photonic lattices is described by a Schrödinger-type equation where propagation distance replaces time [8], leading to the investigation of topological effects in evanescently coupled waveguide arrays [9–11]. In photonic systems, we deal with the bosonic nature of photons, as opposed to the fermionic nature of electrons, requiring new paradigms in the implementation of topology [7], but also allowing new physics.

One-dimensional periodic systems are a particularly simple but powerful example for studying topology effects. Localized modes at the interface of two periodically layered media have long been known [12,13]. However, the topological origin of these interface states has just recently been discussed [14]. The existence of interface states between two one-dimensional photonic crystals (PCs) is rooted in the different bulk band topologies of the respective structures. Topology describes quantities preserved under continuous deformations, defining topological invariants [6]. The band structure of a one-dimensional PC can be continuously deformed by system parameters such as the refractive indices or layer thicknesses, effectively described by the optical path of a unit cell. For an inversion symmetric definition of the unit cell, one can assign a quantized topological number called the Zak phase [14,15] to every band of the band structure, characterizing the spatial distribution of the in-cell periodic Bloch part of the eigenfunctions of the PC. Continuous tuning of system parameters allows one to close and reopen several band gaps. This way, the Zak phase between two bands can be exchanged, which is called band inversion and is an example of a topological transition [14]. In PCs, the band-inverted counterparts show opposite signs of reflection phases. It was consequently proposed to measure topological invariants by phase spectroscopy [16]. The opposite signs of reflection phases allow for topological interface states [14]. The coupling of photonic states located at some material interface can occur in various settings, e.g., at the interfaces of a thin metal film embedded by vacuum or dielectrics [17,18]. Their optical response contains a rich variety of physical phenomena [19]. The concatenation of three PCs with alternating metal-dielectric layers has recently been theoretically discussed [20]. Here, we extend the concept of topological interface states by demonstrating the coupling of topologically confined states theoretically as well as experimentally. We realize a system of coupled interface states showing mode splitting. Both theoretical modeling and experiments show a topological transition for this coupled system. The description of the coupled system is based on a thorough characterization of the substructures relevant for interface states between topologically distinct one-dimensional PCs. We experimentally demonstrate band inversion for the PCs by evaporating metal layers on top of them and measuring the emergence of interface states. The findings are furthermore supported by ellipsometric measurements.

In this way we build up on prior work that experimentally demonstrates interface states in layered systems of titanium dioxide and silicon dioxide together with the measurement of Zak phases [21,22]. The concept was also

*christoph.schmidt6@tu-dresden.de
†karl.leo@tu-dresden.de

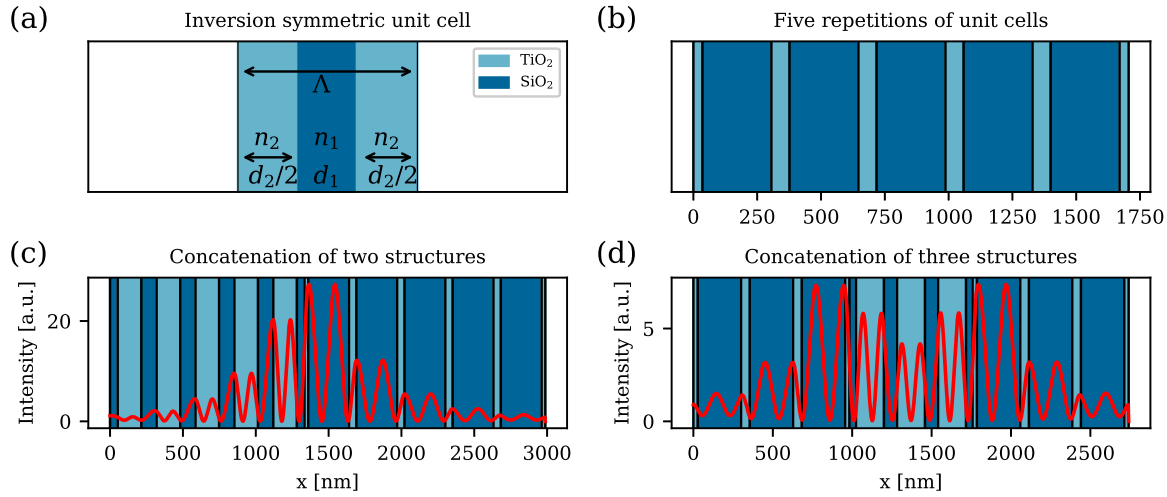

FIG. 1. (a) The inversion symmetric unit cell is the fundamental building block of all of the structures described in this paper. (b) Five repetitions of inversion symmetric unit cells. (c) Concatenation of two structures as in (b) allows for interface states. (d) Concatenation of three structures leads to coupling of interface states.

extended to metal-dielectric structures, showing interface states at the metal-dielectric interface [23], in metadevices [24], and hybrid plasmonic-photonic systems [25]. It was also demonstrated how drastic phase changes appearing in these systems can have interesting device applications, e.g., improving the sensitivity of optical sensors [26].

II. DEVICE ARCHITECTURES

The fundamental building blocks for the devices discussed in this paper are inversion symmetric unit cells as depicted in Fig. 1(a). The infinite repetition of a dielectric unit cell shows a band structure given for propagation perpendicular to the material interfaces by

$$\cos(q\Lambda) = \frac{1}{4n_1n_2}\left[(n_2+n_1)^2\cos\left(\frac{\omega}{c}(\tau_1+\tau_2)\right) - (n_2-n_1)^2\cos\left(\frac{\omega}{c}(\tau_1-\tau_2)\right)\right], \tag{1}$$

with the refractive indices n_i, the thicknesses of the layers d_i, and the corresponding optical path of the layer $\tau_i = n_i d_i$. For a derivation of Eq. (1), see the Supplemental Material [27]. The total optical path of the unit cell reads $\tau = \tau_1 + \tau_2$ and their difference is $\Delta\tau = \tau_1 - \tau_2$. The solutions of Maxwell's equations take the Bloch form $E(x) = E_0(x)e^{-iqx}$ with $E_0(x) = E_0(x+\Lambda)$, where Λ denotes the spatial periodicity of the structure.

The whole frequency range can be divided into two parts called *band gaps* and *bands* and are defined by the absolute value of the right-hand side (rhs) of Eq. (1). If $|\text{rhs}| > 1$, the equation can only be satisfied by purely imaginary q resulting in decaying states. The corresponding finite structure turns out to be very reflective. For $|\text{rhs}| < 1$ we get propagating solutions in the structure. Note that the midgap frequencies ω_m are located at the minima and maxima of rhs, which for small $\frac{\Delta\tau}{\tau}$ is the case at $\sin(\frac{\omega}{c}\tau) = 0$. The mth midgap position is therefore located at [14]

$$\omega_m = m\frac{\pi c}{n_1d_1+n_2d_2} = m\frac{\pi c}{\tau}, \quad \lambda_m = \frac{c}{f_m} = \frac{2\tau}{m}. \tag{2}$$

The midgap frequencies are therefore defined by the total optical path of the unit cell. We can deform the band structure by continuously tuning, e.g., the layer thicknesses of the unit cell.

If we define the thickness of the layer d_2 as a function of the thickness of the layer d_1 in the following way,

$$d_2(d_1) = \frac{1}{n_2}(\tau_0 - n_1\,d_1) = \frac{\tau_0}{n_2} - \frac{n_1}{n_2}d_1 := \beta_0 + \beta_1\,d_1, \tag{3}$$

we always get structures with a constant optical path τ_0, meaning that all of these structures have the same positions of the band gaps. Note that the complete parameter space is covered by $d_1 \in [0, \tau_0/n_1]$ starting by structures where the complete optical path is distributed to n_2 up to structures where the opposite is the case. So if we parametrize this thickness by $d_1 = \delta\frac{\tau_0}{n_1}$, then the whole δ range is covered by $\delta \in [0, 1]$. For this parametrization d_2 reads $d_2 = \frac{\tau_0}{n_2}(1-\delta)$. By sweeping δ along the whole parameter space, several bands close and reopen again. This is called band inversion and results in the exchange of the Zak phases of the respective bands. The value of the Zak phase for a given band is determined by the signs of the reflection phases of the surrounding band gaps [21]. Topologically distinct structures are therefore characterized by the reflection phase throughout this paper. It can be rigorously shown that if the ratio of optical paths $\alpha = \frac{n_1d_1}{n_2d_2} = \frac{m_1}{m_2}$ is a rational number, bands m_1+m_2 and m_1+m_2-1 cross at frequency $\omega_{m_1+m_2} = (m_1+m_2)\frac{\pi c}{n_1d_1+n_2d_2}$ at the center or the boundary of the Brillouin zone [14]. Note that the lowest band is termed the 0th band in this notation.

The devices under investigation consist of a finite number of repetitions of inversion symmetric unit cells with alternating SiO_2 and TiO_2 layers. For fixed refractive indices n_i and a fixed total optical path of the unit cell τ_0, the thicknesses

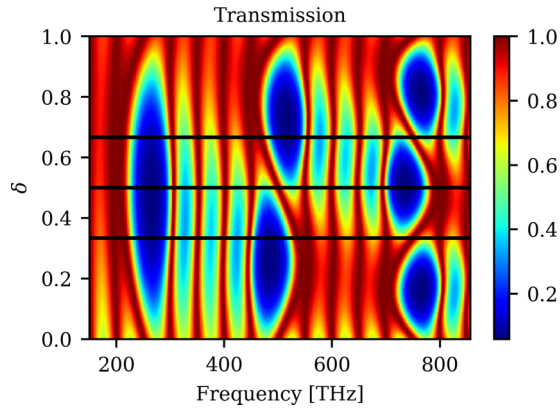

FIG. 2. Transmission of the structure depicted in Fig. 1(b) for a parameter sweep of $\delta \in [0, 1]$ and constant refractive indices.

of the layers in the unit cell d_i are completely determined by the parameter δ. The total device architecture is therefore completely defined by giving the number of repetitions of unit cells, the corresponding δ, and the material that constitutes the outer/inner layer in the unit cell. The main structures described in this paper are summed up in Fig. 1. Note that in the following, increasing δ always corresponds to an increasing thickness of SiO_2 layers.

III. BAND INVERSION

Figure 1(b) shows a repetition of five inversion symmetric unit cells with TiO_2 as the outer layers. The portion of SiO_2 and TiO_2 is controlled by δ as described in the previous section. Figure 2 shows the transmission characteristics of this device for a whole parameter sweep of $\delta \in [0, 1]$. All of the simulations in this paper are conducted by the transfer matrix method. Band closing and therefore band inversion takes place at rational ratios of optical paths of the corresponding layers. The ratio of optical paths reads in our notation $\alpha = \frac{\delta}{(1-\delta)}$, resulting in band crossing, for example, at $\delta \in \{1/3, 1/2, 2/3\}$. The three values of δ are denoted by black horizontal lines and are clearly located at the band inversion points. Other rational ratios lie in higher bands. These data were calculated for constant refractive indices in order to have the black horizontal lines exactly at the band inversion points and have no distortion due to dispersion. This results in the fact that the theory in Figs. 3(a)–3(c) that is calculated with dispersion data for SiO_2 and TiO_2 is not the same as presented in Fig. 2. For the experimental realization, we scaled the system to show band crossing in the green part of the visible spectrum. Hence, the following measurements just show two band gaps in the frequency region of interest. The point of band closing is given by $\delta = 0.5$ for our definition. This corresponds to certain layer thicknesses d_1 and d_2 given by Eq. (3). We evaporated three structures, one of which is located at $\delta < 0.5$, one at $\delta > 0.5$, and one where the bands are exactly closed $\delta = 0.5$. Figures 3(a)–3(c) show the comparison of simulation and measurement of the evaporated samples, which shows good agreement. We first calculated the desired thicknesses in order to fabricate the structures. The mismatch to the actual evaporated structures was taken into account by adjusting the

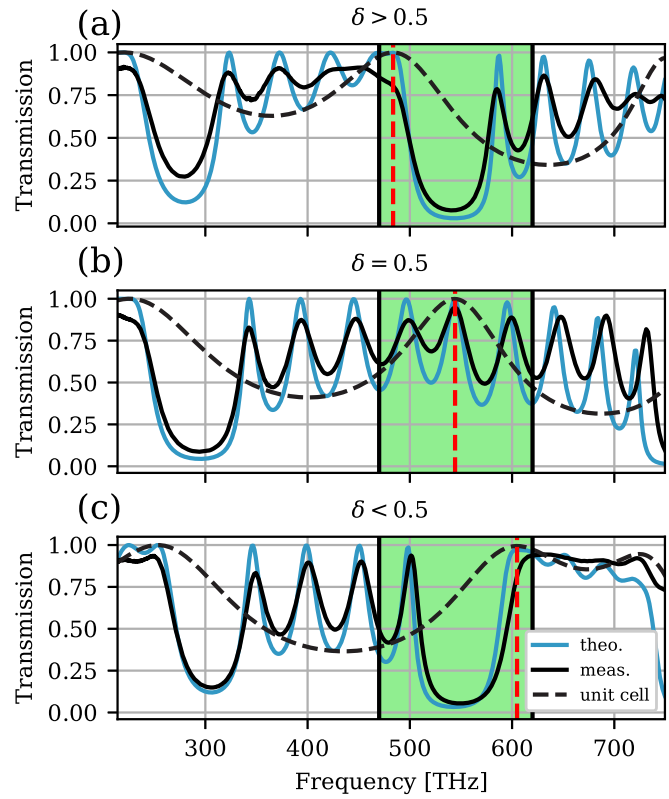

FIG. 3. (a)–(c) Simulated and measured transmittance for different parameters δ. The transmission of the unit cell is depicted by a dashed black line and shows that the band inversion occurs due to a sweep of the unit cell transmission along the band gap for varying δ. The light green shaded area highlights the location of the band gap where the band inversion takes place.

single parameter β_0 in Eq. (3), which basically shifts the midgap positions to the desired location. A general rule of thumb for our samples is that the mismatch gets slightly larger for samples with thick SiO_2 layers, corresponding to $\delta > 0.5$. The band inversion actually takes place due to the fact that the transmission of the unit cell sweeps along the second band gap for a parameter sweep of δ, which is depicted by the red dashed vertical lines in Figs. 3(a)–3(c). This resembles the fact that some information about the optical properties of the infinite bulk or the structure consisting of finite repetitions of unit cells is already contained in the unit cell transmission [28].

IV. METAL-DIELECTRIC INTERFACE STATES

A plasmon polariton state formed at the boundary between a metal and a dielectric Bragg reflector (DBR) is usually called a Tamm state and the mode condition for this state to form reads $r_{\text{metal}} r_{\text{DBR}} = 1$ [29]. The formation of Tamm states at the interface between a semi-infinite one-dimensional PC and a metal for topologically nontrivial samples was recently discussed [30]. Due to the high conductivity of metals, their refractive indices can usually very well be approximated by $n^2 \approx 1 - \omega_p^2/\omega^2$, where the high number of free charge carriers in a metal leads to a plasma frequency ω_p in the far UV region. This gives purely imaginary refractive indices over the

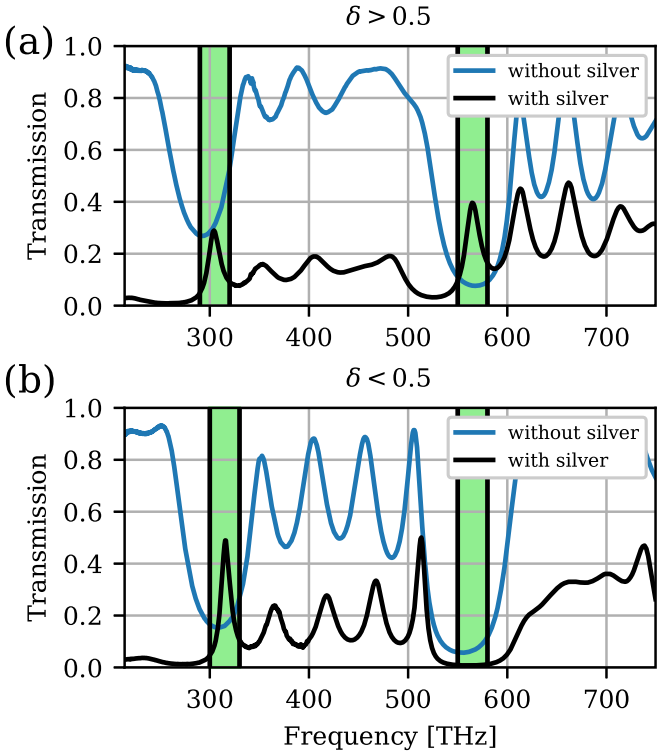

FIG. 4. (a) Measured transmittance for a sample with $\delta > 0.5$ with and without a silver layer on top. (b) Analogous measurement for the sample with $\delta < 0.5$. The light green shaded area highlights the location of the interface state resonances.

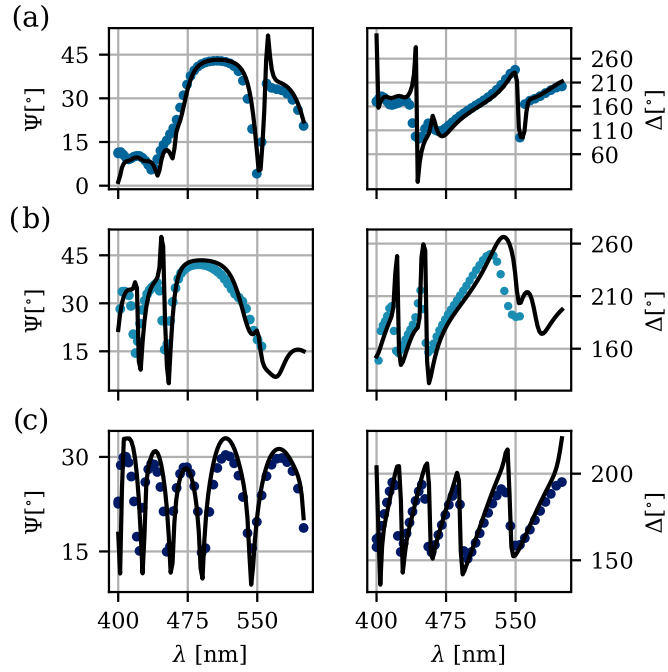

FIG. 5. (a)–(c) Measurement vs theoretical prediction of ellipsometric parameters for the three structures presented in the previous section: (a) $\delta < 0.5$, (b) $\delta > 0.5$, (c) $\delta = 0.5$.

whole visible range, resulting in the same sign of reflection phase for these frequencies. The sign of the reflection phase for the band inverted samples can therefore be checked by evaporating a silver layer on top of the structures and seeing in which band an interface state appears. This is shown in Figs. 4(a) and 4(b).

The transmittances of the structures without the silver layer on top are depicted in blue whereas the measurements of the samples with a silver layer on top are depicted in black. The thickness of the silver layer is 25 nm in both cases. It is clearly visible that for $\delta > 0.5$ we get interface state resonances in both band gaps, whereas for $\delta < 0.5$ we only see an interface state in the lower energy band gap. This indicates that in the higher energy band gap we have opposite signs of reflection phases of the dielectric structures. This leads to the circumstance that if we are concatenating two dielectric structures, which are band inverted counterparts of each other, we should also be able to observe an interface state.

V. REFLECTION PHASES AND ELLIPSOMETRIC MEASUREMENTS

Let the measured ellipsometry parameter of the sample with $\delta > 0.5$ be $\rho_1 = \frac{|r_{p1}|}{|r_{s1}|} e^{i(\theta_{p1}-\theta_{s1})} := \tan\Psi_1 e^{i\Delta_1}$ and of the sample with $\delta < 0.5$ be $\rho_2 = \frac{|r_{p2}|}{|r_{s2}|} e^{i(\theta_{p2}-\theta_{s2})} := \tan\Psi_2 e^{i\Delta_2}$. We conducted ellipsometric measurements for an incident angle of $\theta = 50^\circ$ on the three samples described in Fig. 3. Note that with ellipsometry it is usually not possible to measure absolute values of the reflection phases [31], as the ellipsometric measurements provide the value $\rho = \frac{r_p}{r_s} := \tan(\Psi) e^{i\Delta}$ with the parameters Ψ and Δ. Ψ contains information about a ratio of reflected intensities for p and s polarization translated into an angle, whereas Δ contains information about a difference in reflection phases for p- and s-polarized light. We calculate the wavelength-dependent ellipsometry parameters under the assumption that the layer thicknesses in the simulation presented in Fig. 3 are valid and plot them together with the measured values in Figs. 5(a)–5(c).

Ellipsometry cannot directly measure the absolute values of the reflection phases θ_{pi} and θ_{si}. However, we can explain how the ellipsometric parameters Δ_1 and Δ_2, that we are able to measure, result from the theoretical prediction that shows opposite signs of reflection phases. They are calculated for the structures described in Fig. 3 for an angle of incidence of 50°. The result is presented in Fig. 6(a). The angles actually show opposite signs of the reflection phases as expected, as the corresponding samples are band inverted counterparts of each other. Figure 6(a) shows that for sample 1 the reflection phase for p-polarized light is smaller than the corresponding reflection phase for s-polarized light. Since Δ_1 is the difference of these values, this gives negative values, as can be seen by the black line in Fig. 6(b). The opposite is the case for sample 2, where the reflection phase for p-polarized light is larger than its s-polarized counterpart, resulting in positive values. The red vertical dashed line denotes the point where s- and p-polarized reflection phases are equal, giving a corresponding ellipsometer parameter Δ_2 of zero. The red solid line shows the analogous case for Δ_1.

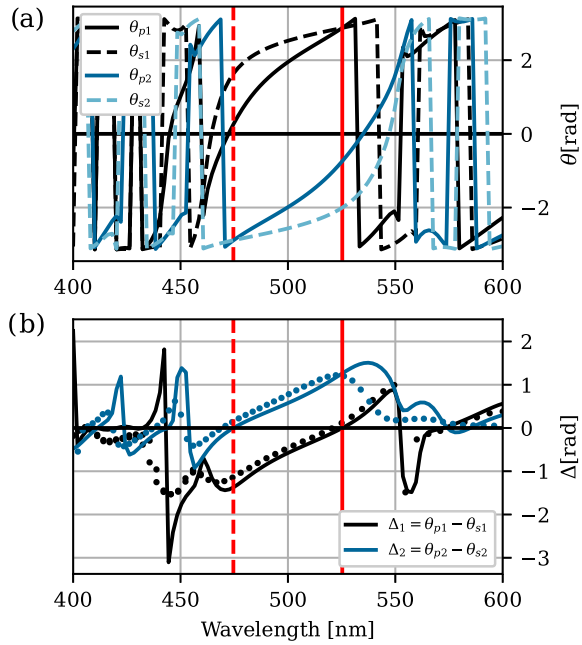

FIG. 6. (a) Calculation of reflection phases of the samples below and above band inversion. (b) Resulting ellipsometric parameters together with measured values.

VI. TOPOLOGICAL INTERFACE STATES

We now consider the optical properties of the concatenation of two structures, each consisting of five unit cells but with different filling ratios δ_l and δ_r. Note that for any (δ_l, δ_r) combination, the two substructures have overlapping midgap positions. We choose a fixed δ_l for the left structure and perform a parameter sweep $\delta_r \in [0, 1]$ for the structure on the right-hand side. We redefine the unit cell of the left structure to have SiO_2 as outer layers such that there exists a real material interface at the boundary of the structures. This changes the Zak phases of the bands but does not change the sign of the reflection phase of the second band gap. See the Supplemental Material for a short proof of why the reflection phase of the second band gap does not change when the unit cell is redefined [27]. This unit cell has a δ_l of 0.24. The corresponding transmission characteristics of the resulting structure are shown in Fig. 7, which reveals that the lowest band shows an interface resonance for the whole parameter space whereas the second band gap shows the emergence of an interface state for $\delta_r > 0.5$, which is the topological transition. We pick two different values of δ_r for the experimental realization, which are approximately represented by the black horizontal lines in Fig. 7, one of which is smaller than 0.5, such that we expect to not observe any interface state in the second band, and one of which is larger than 0.5, such that a topological interface state resonance is expected. This is shown in Figs. 8(a) and 8(b) and indeed we see very good agreement with our theoretical prediction.

Figure 9 shows the frequency-dependent transmission characteristics together with the normalized reflection phases for a finite repetition of five unit cells. The structures described by Figs. 9(a) and 9(b) have TiO_2 as the outer layers. Figure 9(a) corresponds to a material ratio of $\delta = 0.24$

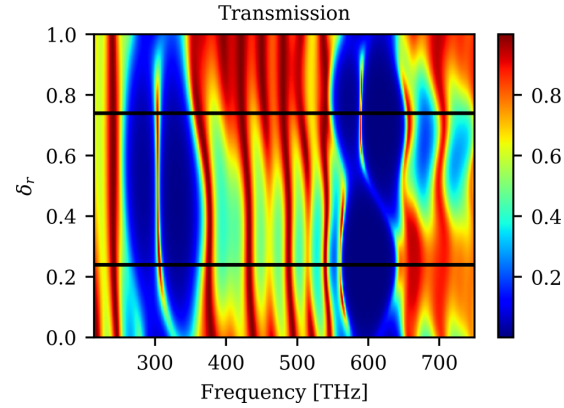

FIG. 7. Transmittance of the structure in Fig. 1(c) for a parameter sweep of δ_r.

whereas Fig. 9(b) has $\delta = 0.74$. Figures 9(c) and 9(d) show the optical properties of structures consisting of five repetitions of unit cells with SiO_2 as the outer layers. Figure 9(c) [Fig. 9(d)] again has a δ of 0.24 (0.74). The white areas are the band gaps of the infinite structure calculated according to the rhs of Eq. (1). Blue areas are the bands, respectively. This figure shows that in the first band for both structures the sign of the reflection phase stays the same for the whole parameter space $\delta \in [0, 1.0]$ and that they have opposite signs. This explains why the interface state in the first gap is present in the whole parameter space. The structures presented in Fig. 8 consist of a fixed structure with SiO_2 layers as the outer layers ($\delta = 0.24$) and a structure with TiO_2 as the outer layers with varying δ. By varying δ, the reflection phase in the second

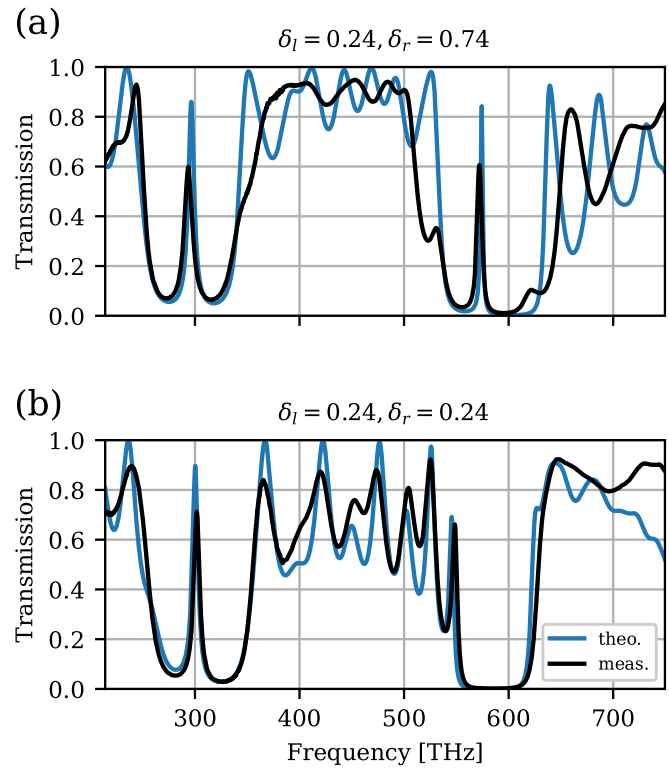

FIG. 8. (a), (b) Measured transmittance of the fabricated samples schematically depicted in Fig. 1(c) compared to theory.

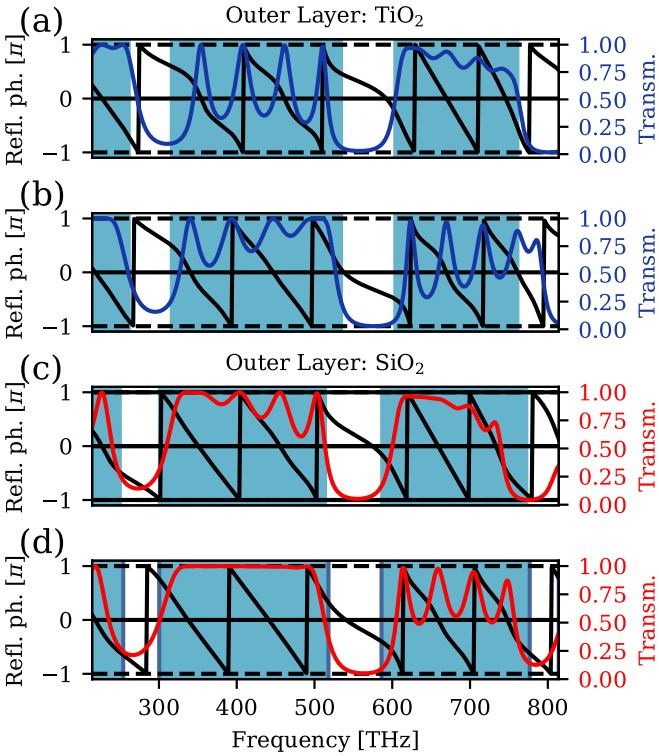

FIG. 9. Frequency-dependent transmission characteristics and normalized reflection phases for structures with TiO_2 [(a) and (b)] and with SiO_2 [(c) and (d)] as outer layers. The structures in (a) and (c) have a δ of 0.24 whereas the structures in (b) and (d) have a δ of 0.74. The light blue areas are bands. White areas are band gaps.

band gap changes its sign due to band inversion. For $\delta < 0.5$ the structures have the same signs of the reflection phases, whereas for $\delta > 0.5$ they have opposite signs, which explains the emergence of a topological interface state.

VII. COUPLED TOPOLOGICAL INTERFACE STATES

The following device is composed of three substructures, each consisting of three unit cells, as depicted in Fig. 1(d). The embedding structures show opposite signs of the reflection phases to the embedded inner structure. This leads to coupling of the interface states and consequently to mode splitting in both of the measured band gaps. Figure 10 shows the transmission for a whole parameter sweep of the inner structure for a fixed $\delta_l = \delta_r = 0.74$ of the outer structures.

The embedded structure consists of three inversion symmetric unit cells with SiO_2 as the outer layers and varying δ_m. According to the argumentation of the previous section and Fig. 9 we have opposite signs of the reflection phases in the second band gap for $\delta_m < 0.5$. This results in mode splitting in both band gaps. For $\delta_m > 0.5$, one of the split modes disappears into the sideband and we are left with a single interface state in the second band gap. We fabricated three coupled systems with $\delta_m \in \{0.24, 0.5, 0.74\}$. The comparison of theory and measurement is shown in Figs. 11(a)–11(c). Note that in order to have good agreement of theory and measurement we again had to scale the theory by varying the parameter β_0 in order to account for tooling changes between fabrication runs. This results in the fact that the theory in Fig. 10 is

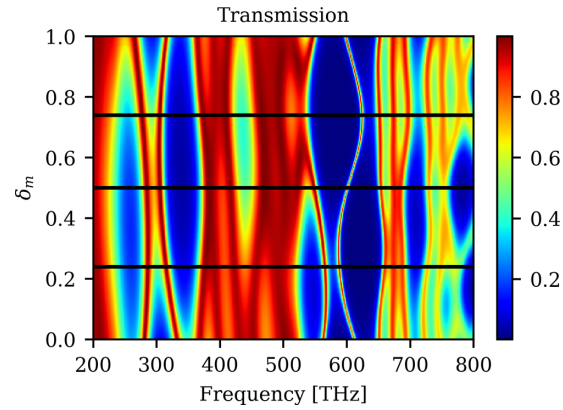

FIG. 10. Transmission of the structure in Fig. 1(d) for a parameter sweep $\delta_m \in [0.0, 1.0]$.

not exactly the same as in Figs. 11(a)–11(c). As reported in previous measurements, we have a larger mismatch for structures with a high portion of SiO_2. The embedding structures actually contain a large amount of SiO_2. For that reason the resonance for $\delta_m = 0.74$ is just residually visible in Fig. 11(c). See the Supplemental Material for further calculations of the transmission characteristics of various coupled systems with different numbers of unit cells [27].

VIII. SUMMARY AND OUTLOOK

We present the experimental realization of a coupled system of topological interface states, consisting of the concatenation of three structures showing mode splitting in both

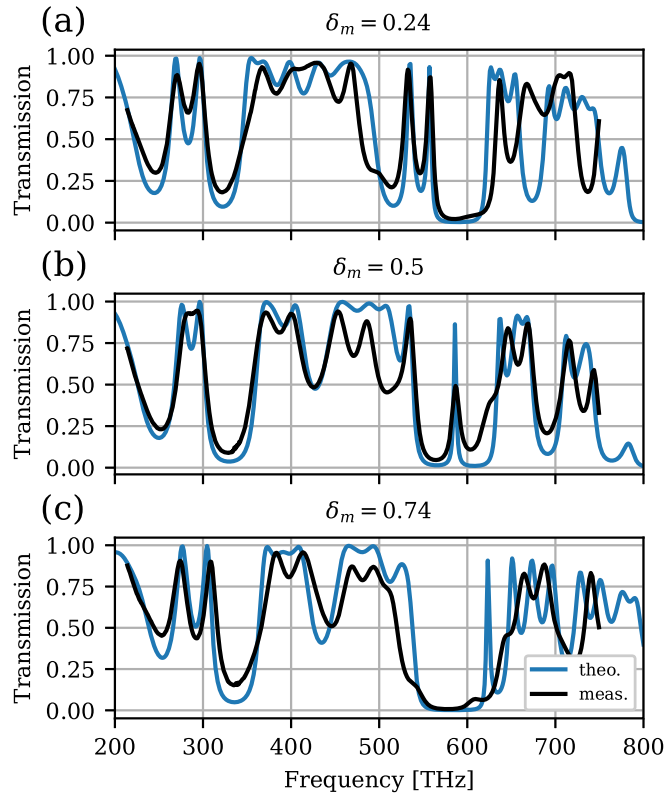

FIG. 11. (a)–(c) Measured transmittance of the fabricated samples schematically depicted in Fig. 1(d) compared to theory.

of the band gaps. We observe a topological transition for that structure, by varying the ratio of SiO_2 and TiO_2 for the embedded structure, that results in the disappearance of the split modes in the second band gap. Our modeling results indicate that the control of the reflection phases by tuning the ratio of optical paths in the unit cell allows for the engineering of photonic states that cannot be equivalently observed in conventional approaches. Standard microcavity approaches are usually given by two distributed Bragg reflectors embedding a cavity layer of an optical thickness of $\lambda/2$. The cavity layer introduces a roundtrip phase shift of 2π, which results in field enhancement in the cavity. The interface states equivalently achieve this by cancellation of the reflection phases of the embedding PCs by having opposite signs. The tunability of the reflection phases by redistribution of the optical path to the constitutive materials adds a new parameter to the system, which basically makes the system asymmetric. This parameter may be used to engineer interfacial states for the benefit of potential applications such as sensors.

IX. EXPERIMENTAL SETUPS

We evaporate layers of SiO_2 and TiO_2 by electron beam evaporation. The electron beam evaporation tool that we are using is called Lab500 and is provided by Leybold Optics. The samples are fabricated on borosilicate glass substrates. The substrates are cleaned with solvents in an ultrasonic bath after which they are placed in a high-vacuum (HV) chamber with a base pressure of 10^{-6} mbar. During the deposition, a partial oxygen pressure of 2×10^{-4} mbar is applied to suppress the formation of other TiO_x/SiO_x compounds. The metal layers were fabricated by thermal evaporation in a UHV chamber system with a base pressure of 10^{-8} mbar. [32]. Transmittance measurements were conducted by UV/VIS spectroscopy with a Shimadzu UV-3100 UV-VIS-NIR recording spectrophotometer. Ellipsometry measurements were conducted with an Accurion EP4 imaging ellipsometer.

ACKNOWLEDGMENTS

We acknowledge financial support from the DFG through the Würzburg-Dresden Cluster of Excellence on Complexity and Topology in Quantum Matter–ct.qmat (EXC 2147, Project-id No. 39085490) and the DFG Projects No. FR 1097/3-1 and No. LE 747/55-1. We thank Jörn Vahland for the help with the evaporation of the metal layers. We thank Prof. Jan Carl Budich for helpful remarks.

[1] C. L. Kane and E. J. Mele, Quantum Spin Hall Effect in Graphene, Phys. Rev. Lett. **95**, 226801 (2005).
[2] M. König, S. Wiedmann, C. Brüne, A. Roth, H. Buhmann, L. W. Molenkamp, X.-L. Qi, and S.-C. Zhang, Quantum spin Hall insulator state in HgTe quantum wells, Science **318**, 766 (2007).
[3] C. L. Kane and E. J. Mele, Z_2 Topological Order and the Quantum Spin Hall Effect, Phys. Rev. Lett. **95**, 146802 (2005).
[4] S. Raghu and F. D. M. Haldane, Analogs of quantum-Hall-effect edge states in photonic crystals, Phys. Rev. A **78**, 033834 (2008).
[5] T. Ozawa, H. M. Price, A. Amo, N. Goldman, M. Hafezi, L. Lu, M. C. Rechtsman, D. Schuster, J. Simon, O. Zilberberg *et al.*, Topological photonics, Rev. Mod. Phys. **91**, 015006 (2019).
[6] L. Lu, J. D. Joannopoulos, and M. Soljačić, Topological photonics, Nat. Photonics **8**, 821 (2014).
[7] M. S. Rider, S. J. Palmer, S. R. Pocock, X. Xiao, P. Arroyo Huidobro, and V. Giannini, A perspective on topological nanophotonics: Current status and future challenges, J. Appl. Phys. **125**, 120901 (2019).
[8] M. C. Rechtsman, J. M. Zeuner, Y. Plotnik, Y. Lumer, D. Podolsky, F. Dreisow, S. Nolte, M. Segev, and A. Szameit, Photonic Floquet topological insulators, Nature (London) **496**, 196 (2013).
[9] J. M. Zeuner, M. C. Rechtsman, Y. Plotnik, Y. Lumer, S. Nolte, M. S. Rudner, M. Segev, and A. Szameit, Observation of a Topological Transition in the Bulk of a Non-Hermitian System, Phys. Rev. Lett. **115**, 040402 (2015).
[10] M. C. Rechtsman, Y. Plotnik, J. M. Zeuner, D. Song, Z. Chen, A. Szameit, and M. Segev, Topological Creation and Destruction of Edge States in Photonic Graphene, Phys. Rev. Lett. **111**, 103901 (2013).
[11] Y. Plotnik, M. C. Rechtsman, D. Song, M. Heinrich, J. M. Zeuner, S. Nolte, Y. Lumer, N. Malkova, J. Xu, A. Szameit *et al.*, Observation of unconventional edge states in "photonic graphene", Nat. Mater. **13**, 57 (2014).
[12] P. Yeh, *Optical Waves in Layered Media* (Wiley, Hoboken, NJ, 2005).
[13] A. V. Kavokin, I. A. Shelykh, and G. Malpuech, Lossless interface modes at the boundary between two periodic dielectric structures, Phys. Rev. B **72**, 233102 (2005).
[14] M. Xiao, Z. Q. Zhang, and C. T. Chan, Surface Impedance and Bulk Band Geometric Phases in One-Dimensional Systems, Phys. Rev. X **4**, 021017 (2014).
[15] J. Zak, Berry's Phase for Energy Bands in Solids, Phys. Rev. Lett. **62**, 2747 (1989).
[16] A. V. Poshakinskiy, A. N. Poddubny, and M. Hafezi, Phase spectroscopy of topological invariants in photonic crystals, Phys. Rev. A **91**, 043830 (2015).
[17] J. Zhang, L. Zhang, and W. Xu, Surface plasmon polaritons: Physics and applications, J. Phys. D **45**, 113001 (2012).
[18] N. Chen, C. Lu, Y. Huang, C. Liao, W. Ke, and B. Huang, Properties of coupled surface plasmon-polaritons in metal-dielectric-metal structures, J. Appl. Phys. **112**, 033111 (2012).
[19] G. Rosenblatt, B. Simkhovich, G. Bartal, and M. Orenstein, Nonmodal Plasmonics: Controlling the Forced Optical Response of Nanostructures, Phys. Rev. X **10**, 011071 (2020).
[20] F. Yang, S. Ma, K. Ding, S. Zhang, and J. B. Pendry, Continuous topological transition from metal to dielectric, Proc. Natl. Acad. Sci. USA **117**, 16739 (2020).
[21] W. S. Gao, M. Xiao, C. T. Chan, and W. Y. Tam, Determination of Zak phase by reflection phase in 1D photonic crystals, Opt. Lett. **40**, 5259 (2015).
[22] W. Gao, M. Xiao, B. Chen, E. Y. Pun, C. T. Chan, and W. Y. Tam, Controlling interface states in 1D photonic crystals by tuning bulk geometric phases, Opt. Lett. **42**, 1500 (2017).

[23] L. Wang, W. Cai, M. Bie, X. Zhang, and J. Xu, Zak phase and topological plasmonic Tamm states in one-dimensional plasmonic crystals, Opt. Express **26**, 28963 (2018).

[24] Q. Wang, M. Xiao, H. Liu, S. Zhu, and C. T. Chan, Measurement of the Zak phase of photonic bands through the interface states of a metasurface/photonic crystal, Phys. Rev. B **93**, 041415(R) (2016).

[25] L. Ge, L. Liu, M. Xiao, G. Du, L. Shi, D. Han, C. T. Chan, and J. Zi, Topological phase transition and interface states in hybrid plasmonic-photonic systems, J. Opt. **19**, 06LT02 (2017).

[26] Y. Tsurimaki, J. K. Tong, V. N. Boriskin, A. Semenov, M. I. Ayzatsky, Y. P. Machekhin, G. Chen, and S. V. Boriskina, Topological engineering of interfacial optical Tamm states for highly sensitive near-singular-phase optical detection, ACS Photonics **5**, 929 (2018).

[27] See Supplemental Material at http://link.aps.org/supplemental/10.1103/PhysRevB.103.085412 for a derivation of Eq. (1), a short proof that the reflection phase of the second band gap does not change, when the unit cell is redefined, as well as further simulations of various coupled systems with different numbers of unit cells per substructure.

[28] P. A. Kalozoumis, G. Theocharis, V. Achilleos, S. Félix, O. Richoux, and V. Pagneux, Finite-size effects on topological interface states in one-dimensional scattering systems, Phys. Rev. A **98**, 023838 (2018).

[29] M. Kaliteevski, I. Iorsh, S. Brand, R. A. Abram, J. M. Chamberlain, A. V. Kavokin, and I. A. Shelykh, Tamm plasmon-polaritons: Possible electromagnetic states at the interface of a metal and a dielectric Bragg mirror, Phys. Rev. B **76**, 165415 (2007).

[30] J. C. G. Henriques, T. G. Rappoport, Y. V. Bludov, M. I. Vasilevskiy, and N. M. R. Peres, Topological photonic Tamm states and the Su-Schrieffer-Heeger model, Phys. Rev. A **101**, 043811 (2020).

[31] H. Tompkins and E. A. Irene, *Handbook of Ellipsometry* (William Andrew, Norwich, NY, 2005).

[32] S. Meister, R. Brückner, M. Sudzius, H. Fröb, and K. Leo, Intracavity metal contacts for organic microlasers, J. Mater. Res. **34**, 571 (2019).